

Flexible Phase Change Materials for Electrically-Tuned Active Absorbers

Jia-Nan Wang, Bo Xiong, Ru-Wen Peng,* Cheng-Yao Li, Ben-Qi Hou, Chao-Wei Chen, Yu Liu, and Mu Wang*

Phase change materials (PCMs), such as GeSbTe (GST) alloys and vanadium dioxide (VO₂), play an important role in dynamically tunable optical metadevices. However, the PCMs usually require high thermal annealing temperatures above 700 K, but most flexible metadevices can only work below 500 K owing to the thermal instability of polymer substrates. This contradiction limits the integration of PCMs into flexible metadevices. Here, a mica sheet is chosen as the chemosynthetic support for VO₂ and a smooth and uniformly flexible phase change material (FPCM) is realized. Such FPCMs can withstand high temperatures while remaining mechanically flexible. As an example, a metal-FPCM-metal infrared meta-absorber with mechanical flexibility and electrical tunability is demonstrated. Based on the electrically-tuned phase transition of FPCMs, the infrared absorption of the metadvice is continuously tuned from 20% to 90% as the applied current changes, and it remains quite stable at bending states. The metadvice is bent up to 1500 times, while no visible deterioration is detected. For the first time, the FPCM metastructures are significantly added to the flexible material family, and the FPCM-based metadevices show various application prospects in electrically-tunable conformal metadevices, dynamic flexible photodetectors, and active wearable devices.

Their phase transition processes can be controlled by external stimuli including thermal,^[1–3] optical,^[4–6] electrical,^[7–9] electrochemical,^[10–13] mechanical,^[14–16] and magnetic^[17,18] approaches. Various dynamic metasurfaces and metadevices have been demonstrated, including dynamic color displays,^[19,20] rewritable data storage,^[21,22] tunable polarizers,^[23,24] waveguide switches,^[25] and reprogrammable holograms.^[26,27] Nevertheless, these PCMs usually require high thermal annealing temperature conditions. For example, the reamorphization of GST requires a thermal annealing process at a temperature in excess of 800 K.^[28,29] The chemosynthesis process of VO₂ usually requires an annealing temperature in excess of 723 K.^[30,31] In consideration of these high-temperature requirements, PCM optical films are usually fabricated on substrates such as glass,^[19,22–24] silicon,^[29] sapphire,^[32] and quartz.^[33] However, all of these substrates are rigid and thus further limit exploration to realize flexible optical metadevices.

1. Introduction

Phase change materials (PCMs), featuring various structural and electronic transitions, play an important role in realizing dynamically tunable metadevices. Owing to their large changes in optical properties, GeSbTe (GST) alloys (Ge₂Sb₂Te₅, Ge₃Sb₂Te₆, etc.) and vanadium dioxide (VO₂) have become the most common PCMs used for tunable optical metadevices.


As we know, flexible optical devices have emerged over the past few decades to provide mechanical flexibility to optical systems.^[34] Owing to the elastic deformability of flexible substrates, these devices can be mechanically deformed (bent, stretched, twisted, compressed, etc.) and work on curved surfaces, inspiring applications such as flexible optical metasurfaces,^[35–37] wearable photonic healthcare devices,^[38] flexible photodetectors,^[39] chemical and biological sensors,^[40,41] and so on. Moreover, mechanical deformation can also be regarded as an extra degree of freedom for optical metasurfaces. By controlling different deformation states of flexible substrates, tunable^[42] and multiplexed^[43] metasurfaces have been demonstrated at visible frequencies. The most widely used flexible substrates are polymer materials such as polydimethylsiloxane (PDMS),^[36] polystyrene (PS),^[37] polyimide (PI),^[38] polyethylene terephthalate (PET),^[39] polyethylene glycol (PEG),^[40] and polycarbonate (PC).^[41] However, owing to thermal instability, these flexible polymer substrates can only operate below the temperature of 500 K,^[44] which is contrary to the above-mentioned high-temperature requirements of PCMs. Very recently, some specific methods have been developed to fabricate PCMs on flexible substrates, such as inkjet-printing PCMs on PI substrates,^[45]

J.-N. Wang, B. Xiong, Prof. R.-W. Peng, C.-Y. Li, B.-Q. Hou, C.-W. Chen, Y. Liu, Prof. M. Wang

National Laboratory of Solid State Microstructures
School of Physics
and Collaborative Innovation Center of Advanced Microstructures
Nanjing University
Nanjing 210093, China

E-mail: rwpeng@nju.edu.cn; muwang@nju.edu.cn

Prof. M. Wang
American Physical Society
Ridge, NY 11961, USA

 The ORCID identification number(s) for the author(s) of this article can be found under <https://doi.org/10.1002/smll.202101282>.

DOI: 10.1002/smll.202101282

fabricating PCMs on thin mica sheets,^[46–52] or utilizing extra buffer layers.^[53,54] However, very few efforts have been devoted to introduce metastructures into such flexible PCM systems to realize flexible and dynamically tunable optical metadevices.

In this work, we intentionally chose a flexible mica sheet as a chemosynthetic support for VO₂, and realized a smooth and uniformly flexible phase change material (FPCM). The mica sheet was atomically smooth and chemically stable, and could endure high temperatures (up to 1373 K for fluorophlogopite mica) and remain highly flexible.^[55,56] The fabricated FPCM exhibited uniform thickness, a homogeneous surface, and excellent mechanical flexibility. The phase transition of the FPCM can be clearly observed in the Raman spectra and absorption spectra in the mid-infrared region. Then, we designed a metal-FPCM-metal (MFM) infrared meta-absorber with high mechanical flexibility and electrical tunability as a metadvice example. An ultra-thin MFM metastructure was introduced as the basic building block. With the electrically-tuned phase transition of the FPCM, the infrared absorption of the metadvice can be continuously tuned by varying the applied current, the functionality of the metadvice changing from that of a perfect absorber to a broadband mirror. Because the magnetic resonance of the surface plasmons excited in

the metastructure is insensitive to the incident angle, the functionality of the metadvice is stable even with a bending radius of 11 mm. To further demonstrate the bending durability of the FPCM-based metadvice, we bent it up to 1500 times, and no visible deterioration could be detected during the bending process. We expect the realization of FPCM based on VO₂ and flexible mica sheet acts as an important candidate for flexible material system. And our study provides a new approach for the design of MFM metadevices with both mechanical flexibility and electric-tunability, which show potential in realizing tunable conformal metadevices, electrically switchable cloaking, dynamically wearable photonic devices, and so on.

2. Results and Discussion

2.1. Electrically-Tuned Flexible Phase Change Material Structure

First, we fabricated an electrically-tuned FPCM structure, as schematically shown in **Figure 1a**. We chose fluorophlogopite mica sheets as the substrate and a 100-nm-thick gold (Au) film was deposited on the substrate by means of magnetron

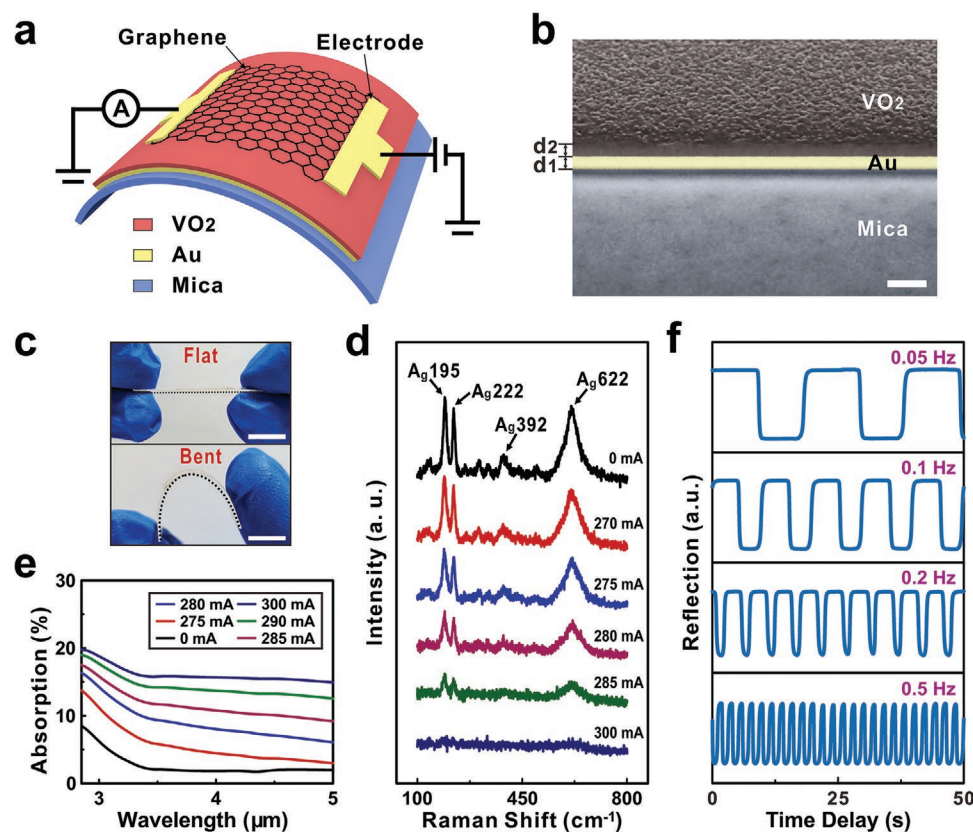


Figure 1. a) Schematic of a flexible and electrically-tuned PCM structure. b) SEM image of a cross-section of the sample without covering the graphene thin film, including mica sheet, 100-nm-thick Au film (d_1), and 100-nm-thick VO₂ film (d_2); the tilted angle for capturing the image is set as 52°; the scale bar is 300 nm. c) The flat state and bent state of the flexible and electrically-tuned PCM. The dashed lines sketch out the outline of the flexible sample; here, the whole sample was placed on a PDMS support for convenient photographing; the scale bars are both 10 mm. d) Raman spectra of the flexible and electrically-tuned PCM when the applied current is from 0 to 300 mA. e) Absorption spectra of the flexible and electrically-tuned PCM structure at wavelengths of 2.85–5 μm measured using an FTIR system when the applied current increases from 0–300 mA. f) Temporal response of the metadvice with the modulation frequency of 0.05, 0.1, 0.2, and 0.5 Hz, respectively.

sputtering. The mica sheet was cleaved repeatedly to realize a satisfactory flexible property when the thickness of the mica sheet was less than 200 μm . Next, the vanadium film was deposited on the Au film by means of electronic beam evaporation (EBE). After annealing in an oxygen atmosphere at the temperature of 430–470 $^{\circ}\text{C}$, a 100-nm-thick VO_2 film working on the flexible substrate could be fabricated to realize the FPCM. Based on the Euler–Bernoulli beam theory,^[57] even the stiff materials can be bent when the film thickness is less than a few hundred nanometers. In this case, the fabricated FPCM naturally possessed high mechanical flexibility. Figure 1b shows the scanning electron microscopy (SEM) image of the cross-section of the FPCM structure. One may find that no pyrolysis or thermal deformation occurred in the mica layer after the high-temperature annealing process in an oxygen atmosphere. Because of the fresh surface of the cleaved sheet, the FPCM exhibited uniform thickness, a homogeneous surface, and high adhesion. It can be seen that the VO_2 film was quite compact and with no cracking.

In order to realize the electrically tunable phase transition of the VO_2 , a pair of “T” shape Au electrodes of 20 nm thickness were fabricated by means of electron beam lithography (EBL) and a subsequent lift-off process after the EBE of the Au film. Subsequently, we transferred a graphene thin film onto the VO_2 film, and a pair of electrodes was set at the two ends of the graphene. Figure 1c shows the mechanical flexibility of the FPCM. Finally, a DC source with a built-in ammeter was connected to the electrodes to accurately apply the electric current to the graphene. The Joule heat generated in the graphene film was able to increase the local temperature above the critical temperature of VO_2 , and thus induced the phase transition of the VO_2 film. In order to demonstrate the electrically-tuned phase transition, we measured the Raman spectra of the FPCM structure when the applied current varied from 0 to 300 mA, as shown in Figure 1d. When no current was applied to the device, several characteristic peaks appeared in the spectrum as A_g modes at 195, 222, 392, and 622 cm^{-1} , respectively, which indicated the monoclinic dielectric phase of VO_2 .^[58,59] Then we increased the current to 275 mA, and these Raman peaks began to decrease, which meant that the VO_2 began to undergo the phase transition. Finally, these peaks would disappear once the current was up to 300 mA, indicating the metallic phase of the VO_2 film.^[58,59] During this phase transition, the refractive index of VO_2 film can also make large changes in the visible and infrared spectrum.^[19,60,61] Figure 1e shows the absorption spectra of the FPCM structure in the mid-infrared region (wavelength from 2.85–5 μm), which was extracted from the reflection data measured using a Fourier-transform infrared (FTIR) system (Vertex 70v, Bruker). The relationship between the reflection and absorption of the sample at a specific wavelength can be expressed as:

$$A(\lambda) = 1 - R(\lambda) - T(\lambda) \quad (1)$$

where A , R , T , and λ represent the absorption, reflection, transmission, and incident wavelengths, respectively. Actually, we have $T(\lambda) \approx 0$ in this structure because of the completely opaque for 100-nm-thick Au film at the wavelengths from 2.85–5 μm , and the graphene film covering on the sample

makes a negligible influence on the absorption spectra of the FPCM structure (Part I, Supporting Information). It can be seen in Figure 1e that the absorption can be continuously tuned when the applied current increases from 285 to 300 mA, indicating the electrical tunability of the FPCM structure. In addition, the time response of this device was also examined based on the time-domain reflection measurement. As shown in Figure 1f, the measured ON and OFF switching times for 0.1 Hz pulsed square-wave current were ≈ 330 and ≈ 620 ms, respectively. More details are discussed in Part II, Supporting Information.

2.2. Design the Metal-FPCM-Metal Infrared Meta-Absorber with Mechanical Flexibility

Based on the FPCM, we designed an MFM infrared meta-absorber with electrical tunability, high mechanical flexibility, and good bending durability. The Au nanodisk array was designed on the smooth surface of the FPCM, resulting in an MFM metastructure, as schematically shown in Figure 2a. The thickness of the Au nanodisk array was 20 nm and the diameter of each nanodisk was 425 nm. The Au nanodisk array had a period of 700 nm along both x - and y - directions. The absorption spectra of the sample when the VO_2 film was in the dielectric and metallic phases were then simulated using the finite-difference time-domain method (a commercial software from Lumerical Inc., FDTD Solutions), as shown in Figure 2b. When the VO_2 film was in the dielectric phase, there was a distinct absorption peak at a wavelength of approximately 3.5 μm . Here, near 100% absorption of the metadvice could be obtained, demonstrating a perfect absorber at a specific wavelength. Nevertheless, when the VO_2 film transferred to the metallic rutile phase, the absorption of the metadvice decreased to approximately 20% at the wavelengths from 2–5 μm , which indicated a broadband mirror in the mid-infrared region.

In order to better understand the underlying mechanism of the metadvice, we simulated the magnetic field distributions at 3.5 μm . Figure 2c shows the magnetic field intensity distributions when the VO_2 film was in the dielectric phase in the x - z (left panel) and x - y planes (right panel), respectively. In this case, the top Au nanodisk array, the middle VO_2 film, and the bottom Au reflected layer formed a typically metal-insulator-metal configuration. It is clear that the magnetic field was concentrated mainly inside the VO_2 film when light was incident in the x -polarized direction, indicating the excitation of magnetic resonance. At the resonance, the metadvice will strongly interact with the magnetic field of the incident light. And the localized enhanced electromagnetic field can greatly increase the Ohmic loss^[62,63] and therefore gives rise to a distinct absorption peak in the spectrum. In this situation, almost no light radiated to the far-field, as shown in Part III, Supporting Information; therefore, the sample acts as a perfect absorber at this wavelength. However, if the VO_2 film turns into the metallic phase, because of the variation in the refractive index of the VO_2 film, the resonant mode of the Au nanodisk would change significantly. Figure 2d shows the magnetic field intensity distributions around the Au nanodisk at a wavelength of 3.5 μm

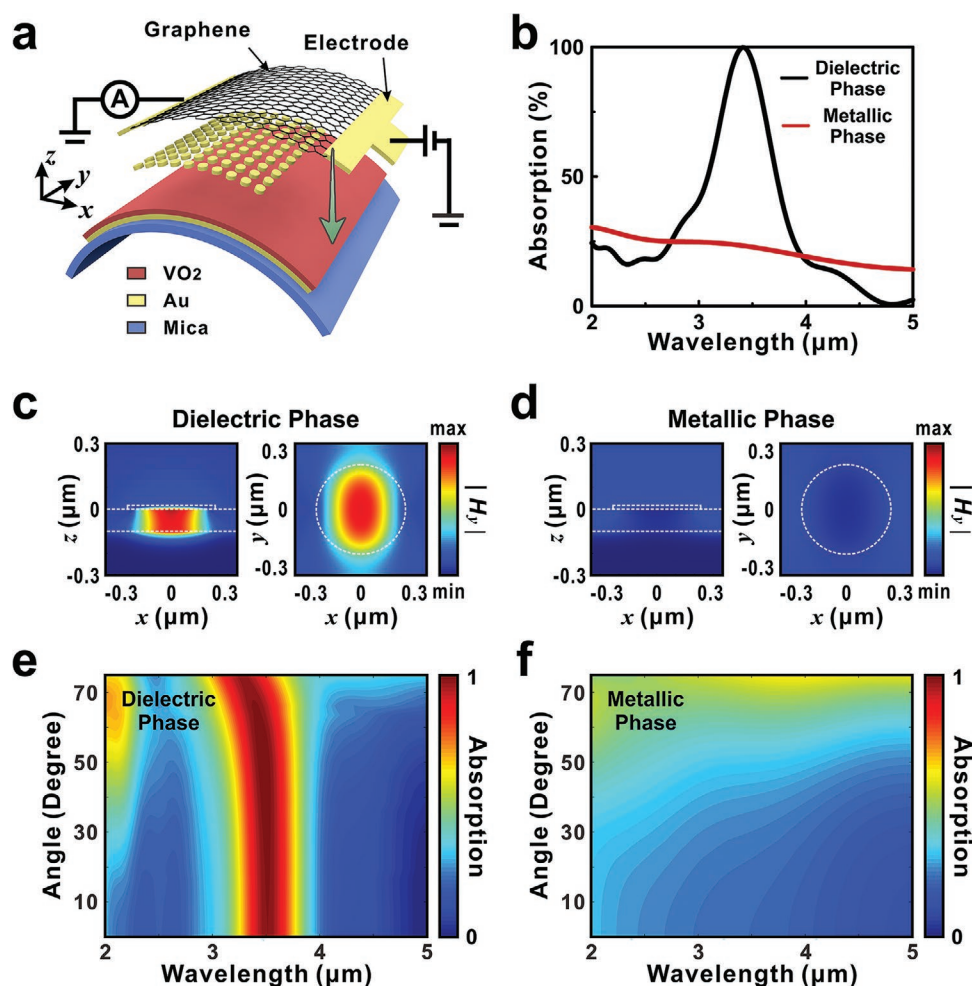


Figure 2. a) Schematic of a flexible and electrically-tuned infrared meta-absorber, in which a metastructure of Au nanodisk array is inserted into the flexible and electrically-tuned PCM between the VO₂ film and graphene thin film. b) Simulated absorption spectra of the flexible and electrically-tuned infrared meta-absorber at wavelengths of 2–5 μm when the VO₂ film is at the dielectric phase and metallic phase. The magnetic field intensity distributions around the Au nanodisk at an incident wavelength of 3.5 μm in the *x*-*z* and *x*-*y* planes when the VO₂ film is at c) dielectric phase and d) metallic phase. The white dashed lines indicate the structure profiles of the building block. The simulated absorption spectra for the incident light at different incident angles when the VO₂ film is at e) dielectric phase and f) metallic phase.

when the VO₂ film was in the metallic phase in the *x*-*z* (left panel) and *x*-*y* planes (right panel), respectively. Under these circumstances, almost no magnetic field was concentrated and most of the light was reflected to the far-field, as shown in Part III, Supporting Information.

Further, we found that because the excited magnetic resonance is insensitive to the incident angle, the meta-absorber exhibited consistent functionality in different bending states. This wide-angle of acceptance is one of the most significant features of a flexible device. Figure 2e,2f depicts the simulated absorption spectra of the metadvice at different incident angles in the *x*-*z* plane. It is clear that the variation in the absorption was negligible even under an oblique incidence angle of 50° when the VO₂ film was in the dielectric phase, indicating a perfect absorber with a wide angle of acceptance. Moreover, owing to the rotation symmetry of the Au nanodisk, this flexible and dynamically tunable infrared meta-absorber could work for any arbitrary polarization states.

2.3. Electrical Tunability of the MFM Infrared Meta-Absorber

Based on the simulation results mentioned above, we fabricated the metastructure of the 20-nm-thick Au nanodisk array on the FPCM structure. The design of the FPCM structure was the same as that shown in Figure 1a, consisting of a mica sheet, Au film, and VO₂ film, from bottom to top. The nano-fabrication process is as following: First, a resist layer was spin-coated on the FPCM structure. Then the sample was loaded into the EBL system for electron-beam exposure. After the exposure, the sample was developed and a 20-nm-thick Au film was subsequently deposited on the sample by means of EBE. Then, a 20-nm-thick Au nanodisk array was fabricated on the FPCM structure after a lift-off process. Subsequently, a pair of “T” shape Au electrodes of 20 nm thickness were also fabricated at the adjacent sides of the metastructure. Finally, a graphene thin film was transferred onto the Au nanodisk array and the two ends of the graphene were in contact with

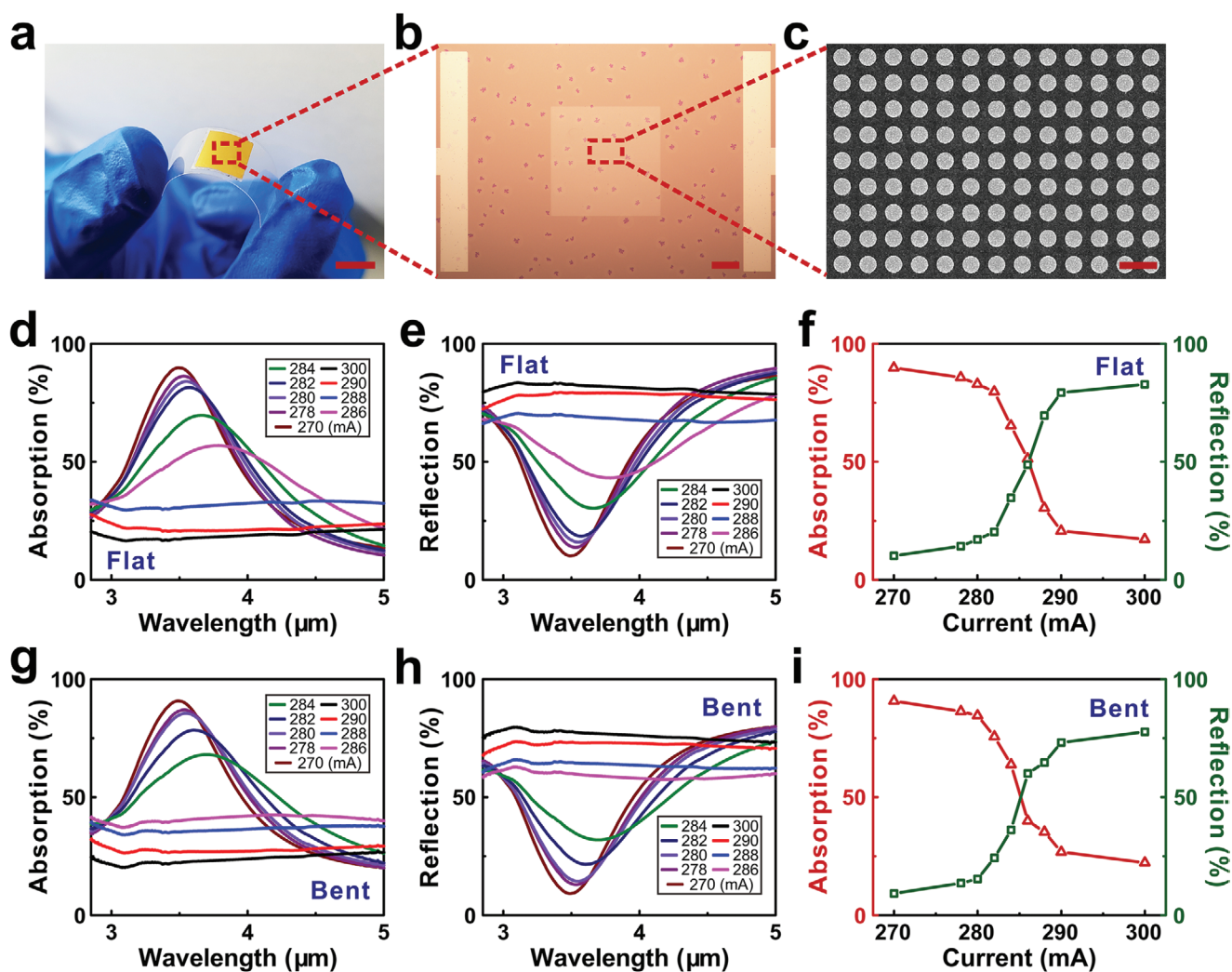


Figure 3. a) Photograph of the flexible and electrically-tuned infrared meta-absorber. Here, the meta-device was placed on a PDMS support for convenient photographing; the scale bar is 10 mm. b) Micrograph of the flexible and electrically-tuned infrared meta-absorber, where the metastructure is in the middle of the graph and a pair of Au electrodes are fabricated at the left and right sides of the metastructure; the scale bar is 50 μm . c) SEM image of the Au nanodisk array with nanodisk of diameter 425 nm and period 700 nm; the scale bar represents 1 μm . Measured d) absorption spectra and e) reflection spectra of the flexible and electrically-tuned infrared meta-absorber at wavelengths of 2.85–5 μm when the meta-device is in a flat state as the applied current increases from 270–300 mA. f) The variation of the absorption and reflection of the meta-device at a wavelength of 3.48 μm as a function of applied current when the meta-device is in a flat state. Measured g) absorption spectra and h) reflection spectra of the flexible and electrically-tuned infrared meta-absorber at wavelengths of 2.85–5 μm when the meta-device is in a bent state (here the bending radius is 23 mm) as the applied current increases from 270–300 mA. i) The variation of the absorption and reflection of the meta-device at a wavelength of 3.48 μm as a function of applied current when the meta-device is in a bent state.

the electrodes to establish a circuit to the external DC source. The flexibility of the meta-device was pretty good, as shown in **Figure 3a**. The entire region of the Au nanodisk array was a square with an edge length of 200 μm , as can be seen in the optical image shown in **Figure 3b**. It can also be seen that the Au electrodes were set on both sides of the Au nanodisk array, the distance from the edge of the Au nanodisk array to the Au electrode being 200 μm . **Figure 3c** shows the details of the Au nanodisk array on the VO_2 film with a nanodisk diameter of 425 nm and a period of 700 nm.

Now we carried out the optical measurements of the MFM meta-device at applying different currents. First, we set the applied current to 270 mA (or lower, even without applied

current)—the VO_2 film always maintains a dielectric phase under these conditions. We measured the reflection spectrum and extracted the absorption spectrum using Equation (1) at wavelengths from 2.85 to 5 μm when the meta-device was in the flat state. The black lines plotted in **Figure 3d,e** represent the measured absorption and reflection spectra, respectively. It can be seen that there was an obvious absorption peak at a wavelength of approximately 3.48 μm , and the absorption of the meta-device was close to 90%, indicating an infrared absorber at this wavelength. Followed by this, we adjusted the applied current to 300 mA—it is well-known that the VO_2 film is able to undergo a phase transition from the dielectric phase to the metallic phase, as shown in **Figure 1e**. As a result, the

absorption of the sample significantly reduced to approximately 20% and the reflection increased to approximately 80% at any wavelength from 2.85 to 5 μm , which can be seen from the brown lines in Figure 3d,3e, indicating a broadband mirror under this condition. One may find that the measured spectra at the applied current of 270 and 300 mA were in good agreement with the simulation results shown in Figure 2b.

To investigate the intermediate states of the phase transition, we also measured the reflection and absorption spectra of the sample at several discrete currents ranging from 270 to 300 mA, and the measured results are shown in Figure 3d,3e. Based on the accuracy of the electrical tunability, several stable intermediate states of the reflection and absorption spectra could be obtained. It can be seen that when the applied current increased, the peak position red-shifted and the absorption at a wavelength of 3.48 μm decreased gradually. Figure 3f shows the variation of the absorption and reflection at a wavelength of 3.48 μm as a function of the applied current. The sample obtained approximately 70% variation of the absorption and reflection when the applied current increased from 270 to 300 mA, indicating an infrared meta-absorber with continuous electrical tunability and a wide modulation range. Moreover, it should be mentioned that the absorption of the metadvice could form an obvious hysteresis in this modulation range, which demonstrated the electrical tunability was fully reversible (Part IV, Supporting Information).

Subsequently, we applied stress to the mica substrate from both sides toward the middle, and thus the entire metadvice was squeezed into a bent state. In the case that the bending radius is 23 mm, we measured the reflection and absorption spectra of the sample when the applied current increased from 270 to 300 mA, the results of which are shown in Figure 3g,h. The variation of the absorption and reflection at a wavelength of 3.48 μm as a function of applied current is shown in Figure 3i, which demonstrates fairly good continuous electrical tunability. It is obvious that the variant trends of the absorption and reflection spectra in the bent state were consistent with those in the flat state, and they could also form a typical hysteresis as mentioned above (Part IV, Supporting Information). All these experimental results state that the electrically-tuned meta-absorber worked pretty well even in the bent states.

2.4. Mechanical Flexibility and Bending Durability of the Electrically-Tuned Infrared Meta-Absorber

Next, we demonstrated the mechanical flexibility of the electrically-tuned MFM infrared meta-absorber by bending the mica substrate to various radii. The bending radius (r) satisfies the equation:

$$d = 2r \sin \frac{l}{2r} \quad (2)$$

where d and l represent the measured chord length and side length of the mica substrate, respectively. First, we kept the applied current being zero, that is, disconnecting the sample with the external DC source. In this case, the sample acted as a flexible absorber based on the dielectric phase of the VO_2

film. Figure 4a shows the absorption spectra of the metadvice with different bending radii extracted from the measured reflection spectra in Part V, Supporting Information. Here, the detected area entirely covered the whole region of meta-structure. Actually, the absorption spectra remained almost the same at different positions of a bent meta-absorber regardless of the change of incident angle. The detailed experimental data and discussions on this aspect are given in Part VI, Supporting Information. A negligible variation in the absorption spectrum could be observed even the bending radius reached 11 mm. When the bending radius decreased to 10 mm, the absorption spectrum declined and the absorption peak blue-shifted slightly. This tendency was consistent with the simulated results as shown in Figure 2e. The absorption at a wavelength of 3.48 μm as a function of bending radius is also plotted as the red line in Figure 4b. The absorption was maintained at approximately 90% even the bending radius reached 11 mm. However, it exhibited a small reduction when the bending radius was less than 10 mm.

Subsequently, we connected the sample to the DC source and set the applied current to 300 mA. In this situation, the VO_2 film was in the metallic phase and the metadvice acted as a flexible broadband mirror. Figure 4c shows the absorption spectra of the metadvice with different bending radii extracted from the measured reflection spectra in Part V, Supporting Information. The absorption at a wavelength of 3.48 μm as a function of bending radius is plotted as the blue line in Figure 4b. The absorption continuously increased without any significant changes at different bent states, which was also consistent with the simulated results of Figure 2f. To further analyze the mechanical flexibility of the electrically-tuned infrared meta-absorber, we plotted the relative absorption change ($|\Delta A/A|$) as a function of bending radius, which is defined as:

$$|\Delta A/A| = \frac{|A(I_2) - A(I_1)|}{A(I_1)} \times 100\% \quad (3)$$

where $A(I_1)$ and $A(I_2)$ represent the absorption when the VO_2 film is at dielectric phase and metallic phase, respectively. To satisfy the phase change condition, here we set $I_1 = 0$ and $I_2 = 300$ mA in the experiment and the measured results are shown in Figure 4d. It is clear that $|\Delta A/A|$ at a wavelength of 3.48 μm was maintained at approximately 86% even with a bending radius of 11 mm, which demonstrates the stable mechanical flexibility of the metadvice.

The bending durability is also particularly important for flexible devices, and it is a primary index of device degradation. Here, the flexible and electrically-tuned infrared meta-absorber was fixed onto a mechanical bending machine and bent for 1500 times (from flat to a bending radius of 11 mm). Figure 5a,b shows the absorption spectra at different bending cycles when the applied current was 0 and 300 mA, respectively, which were extracted from the measured reflection spectra in Part VII, Supporting Information. We also plotted the absorption and reflection at the wavelength of 3.48 μm when the bending cycles vary from 0 to 1500 times, as shown in Figure 5c,d. In both cases, no visible deterioration was measured in absorption or reflection even after the 1500-cycle bending test. To better analyze

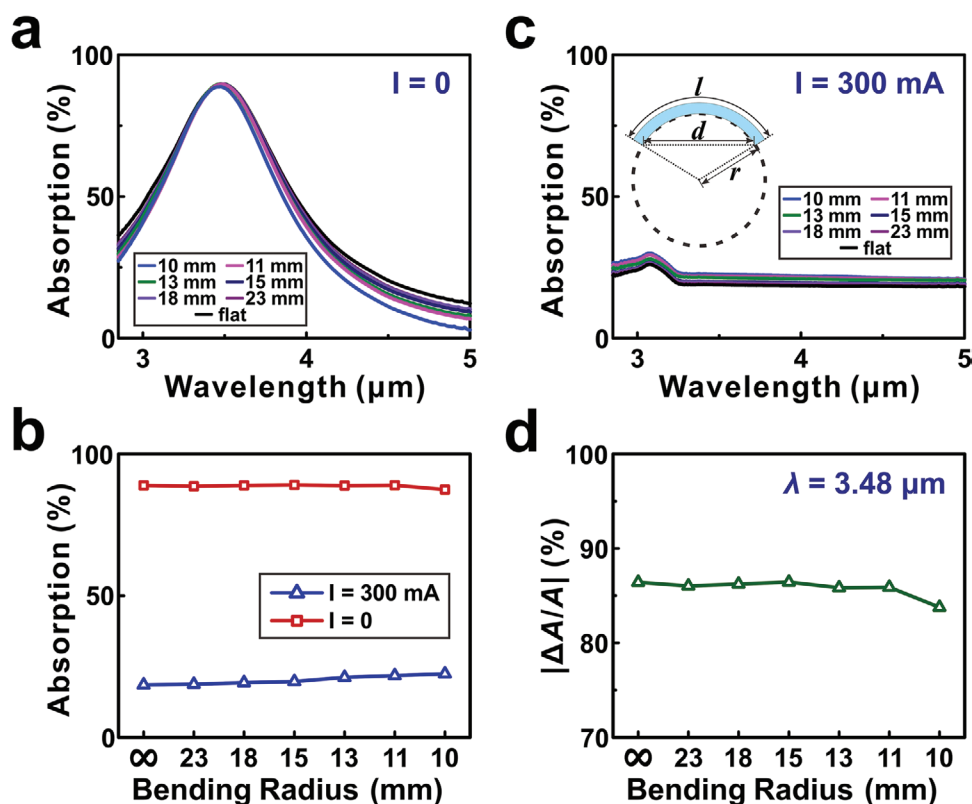


Figure 4. a) Measured absorption spectra of the flexible and electrically-tuned infrared meta-absorber under a flat state and different bent states with bending radii from 23–10 mm when the applied current is 0. b) Measured absorption of the metadvice at a wavelength of 3.48 μm as a function of bending radius when the applied current is 0 and 300 mA. c) Measured absorption spectra with bending radii from 23–10 mm when the applied current is 300 mA. Inset: Schematic of the bending process, where the blue layer represents the mica sheet layer, and r , l , and d represent the bending radius, side length of the mica sheet, and chord length, respectively. The bending radius is solved by the equation $d = 2r \sin(l/2r)$. d) The relative absorption change ($|\Delta A/A|$) of the metadvice at 3.48 μm wavelength as a function of bending radius, where the relative absorption change is defined as $|\Delta A/A| = |A(I_2) - A(I_1)|/A(I_1) \times 100\%$, where $A(I_1)$ and $A(I_2)$ represent the absorption when the VO_2 film is at dielectric phase and metallic phase, respectively. Here, we set $I_1 = 0$ and $I_2 = 300$ mA.

the bending durability of the metadvice, we plotted $|\Delta A/A|$ at a wavelength of 3.48 μm as a function of bending cycles, as shown in Figure 5e. It is clear that the $|\Delta A/A|$ remained stable during the bending process and no indication of metadvice degradation occurred, which demonstrated that the flexible and electrically-tuned infrared meta-absorber has stable electrical tunability yielded outstanding bending durability. We also took the SEM images of the device after different bending cycles and no obvious cracking or structural shedding had been observed even after 1500 times (Part VIII, Supporting Information). These results indicated good structural stability of the FPCM-based metadivices during the bending processes.

It is worthwhile to mention that this meta-absorber based on FPCM works at the wavelengths from 2.85 to 5 μm . This operation band located at the region of mid-infrared atmospheric transparency window (3–5 μm), playing an important role in astronomical observation, environmental monitoring, daytime radiative cooling, and so on.^[64,65] We anticipate that such flexible and electrically-tuned meta-absorber may introduce significant inspirations to the applications such as dynamic infrared remote sensing, flexible thermal emitters, and tunable radiative cooling device.

3. Conclusions

To summarize, by introducing cleaved mica sheets as the chemosynthetic support for VO_2 , we realized a smooth and uniform FPCM. Unlike traditional polymer substrates, this flexible mica sheet is atomically smooth and high-temperature stable, which can endure the high temperatures required during the annealing process of VO_2 . The fabricated FPCM exhibited uniform thickness, a homogeneous surface, and excellent mechanical flexibility. Then by using the graphene layer, a precise and continuous electrical control was achieved for the phase transition process of FPCM. Further, based on this FPCM we designed a flexible and electrically-tuned infrared meta-absorber. An ultrathin MFM structure was introduced as the basic building block. The infrared absorption of the metadvice can be continuously tuned from 20% to 90% by varying the applied current in graphene. Because the magnetic resonance excited in the metastructure is insensitive to the incident angle, the functionality of the metadvice was stable even at the bending states. Finally, to demonstrate the bending durability of the metadvice, we bent it up to 1500 times, where no visible deterioration could be detected. It is worth mentioning that the metadvice is designed to work at

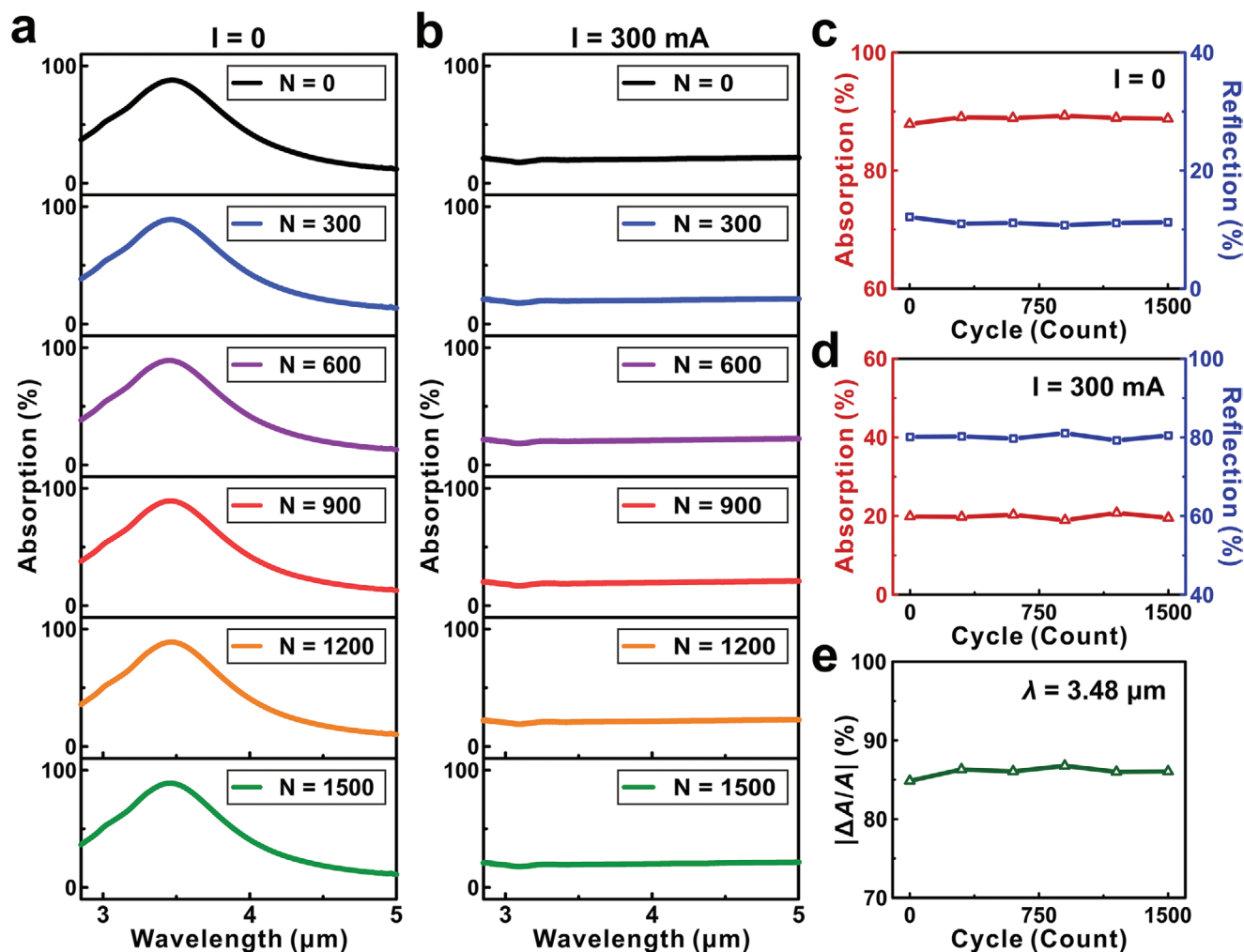


Figure 5. The absorption spectra at different bending cycles when the applied current was a) 0 and b) 300 mA, respectively. The absorption and reflection at 3.48 μm are plotted as a function of the bending cycles at the applied current state of c) 0 and d) 300 mA. No visible deterioration was measured in absorption or reflection even after the 1500-cycle bending test. e) The relative absorption change ($|\Delta A/A|$) at 3.48 μm wavelength of the metamaterial is plotted as a function of the bending cycles.

the mid-infrared atmospheric transparency window, which may have inspirations to thermal emission devices, infrared remote sensing, radiative cooling, etc. We suggest that our study on the FPCM metastructures has significantly promoted the application of phase change materials to the flexible metamaterial family, and the FPCM-based metamaterials may lead to various applications in electrically-tunable conformal metamaterials, dynamic flexible photodetectors, and active wearable devices.

Supporting Information

Supporting Information is available from the Wiley Online Library or from the author.

Acknowledgements

This work was supported by the National Key R&D Program of China (2020YFA0211300, 2017YFA0303702), and the National Natural Science Foundation of China (Grant Nos. 11634005, 61975078, and 11974177).

Conflict of Interest

The authors declare no conflict of interest.

Data Availability Statement

Research data are not shared.

Keywords

flexible and electrically-tuned metamaterials, flexible electrically-tuned infrared meta-absorber, flexible phase change materials

Received: March 3, 2021

Revised: April 25, 2021

Published online:

[1] F. J. Morin, *Phys. Rev. Lett.* **1959**, 3, 34.

[2] Z. Yang, C. Ko, S. Ramanathan, *Annu. Rev. Mater. Res.* **2011**, 41, 337.

- [3] K. Liu, S. Lee, S. Yang, O. Delaire, J. Wu, *Mater. Today* **2018**, *21*, 875.
- [4] M. Liu, H. Y. Hwang, H. Tao, A. C. Strikwerda, K. Fan, G. R. Keiser, A. J. Sternbach, K. G. West, S. Kittiwatanakul, J. Lu, S. A. Wolf, F. G. Omenetto, X. Zhang, K. A. Nelson, R. D. Averitt, *Nature* **2012**, *487*, 345.
- [5] O. L. Muskens, L. Bergamini, Y. Wang, J. M. Gaskell, N. Zabala, C. H. de Groot, D. W. Sheel, J. Aizpurua, *Light: Sci. Appl.* **2016**, *5*, e16173.
- [6] D. Y. Lei, K. Appavoo, F. Ligmajer, Y. Sonnefraud, R. F. Haglund Jr., S. A. Maier, *ACS Photonics* **2015**, *2*, 1306.
- [7] S. D. Ha, Y. Zhou, C. J. Fisher, S. Ramanathan, J. P. Treadway, *J. Appl. Phys.* **2013**, *113*, 184501.
- [8] L. Fan, Y. Chen, Q. Liu, S. Chen, L. Zhu, Q. Meng, B. Wang, Q. Zhang, H. Ren, C. Zou, *ACS Appl. Mater. Interfaces* **2016**, *8*, 32971.
- [9] J. del Valle, P. Salev, F. Tesler, N. M. Vargas, Y. Kalcheim, P. Wang, J. Trastoy, M. H. Lee, G. Kassabian, J. G. Ramirez, M. J. Rozenberg, I. K. Schuller, *Nature* **2019**, *569*, 388.
- [10] M. Nakano, K. Shibuya, N. Ogawa, T. Hatano, M. Kawasaki, Y. Iwasa, Tokura, *Appl. Phys. Lett.* **2013**, *103*, 153503.
- [11] D. Li, A. A. Sharma, D. K. Gala, N. Shukla, H. Paik, S. Datta, D. G. Schlom, J. A. Bain, M. Skowronski, *ACS Appl. Mater. Interfaces* **2016**, *8*, 12908.
- [12] C. J. Dahlman, G. LeBlanc, A. Bergerud, C. Staller, J. Adair, D. J. Milliron, *Nano Lett.* **2016**, *16*, 6021.
- [13] S. Chen, Z. Wang, H. Ren, Y. Chen, W. Yan, C. Wang, B. Li, J. Jiang, C. Zou, *Sci. Adv.* **2019**, *5*, eaav6815.
- [14] J. Cao, Y. Gu, W. Fan, L. Q. Chen, D. F. Ogletree, K. Chen, N. Tamura, M. Kunz, C. Barrett, J. Seidel, J. Wu, *Nano Lett.* **2010**, *10*, 2667.
- [15] B. Hu, Y. Ding, W. Chen, D. Kulkarni, Y. Shen, V. V. Tsukruk, Z. L. Wang, *Adv. Mater.* **2010**, *22*, 5134.
- [16] B. Hu, Y. Zhang, W. Chen, C. Xu, Z. L. Wang, *Adv. Mater.* **2011**, *23*, 3536.
- [17] J. Choi, B. J. Kim, G. Seo, H. T. Kim, S. Cho, Y. W. Lee, *Curr. Appl. Phys.* **2016**, *16*, 335.
- [18] D. Singh, C. S. Yadav, B. Viswanath, *Mater. Lett.* **2017**, *196*, 248.
- [19] F. Z. Shu, F. F. Yu, R. W. Peng, Y. Y. Zhu, B. Xiong, R. H. Fan, Z. H. Wang, Y. M. Liu, M. Wang, *Adv. Opt. Mater.* **2018**, *6*, 1700939.
- [20] N. Frank, X. Y. Duan, N. Liu, *Sci. Adv.* **2020**, *6*, eabc2709.
- [21] Z. M. Sun, J. Zhou, R. Ahuja, *Phys. Rev. Lett.* **2007**, *98*, 055505.
- [22] N. Youngblood, C. Ríos, E. Gemo, J. Feldmann, Z. G. Cheng, A. Baldycheva, W. H. Pernice, C. D. Wright, H. Bhaskaran, *Adv. Funct. Mater.* **2019**, *29*, 1807571.
- [23] Z. Y. Jia, F. Z. Shu, Y. J. Gao, F. Cheng, R. W. Peng, R. H. Fan, Y. Liu, M. Wang, *Phys. Rev. Appl.* **2018**, *9*, 034009.
- [24] Y. P. Song, P. P. Xu, *Opt. Commun.* **2018**, *426*, 30.
- [25] A. Joushaghani, J. Jeong, S. Paradis, D. Alain, J. S. Aitchison, J. K. S. Poon, *Opt. Express* **2015**, *23*, 3657.
- [26] F. Zhang, X. Xie, M. B. Pu, Y. H. Guo, X. L. Ma, X. Li, J. Luo, Q. He, H. L. Yu, X. G. Luo, *Adv. Mater.* **2020**, *32*, 1908194.
- [27] X. B. Liu, Q. Wang, X. Q. Zhang, H. Li, Q. Xu, Y. H. Xu, X. Y. Chen, S. X. Li, M. Liu, Z. Tian, C. H. Zhang, C. W. Zou, J. G. Han, W. L. Zhang, *Adv. Opt. Mater.* **2019**, *7*, 1900175.
- [28] M. Wuttig, H. Bhaskaran, T. Taubner, *Nat. Photonics* **2017**, *11*, 465.
- [29] Y. R. Qu, Q. Li, K. K. Du, L. Cai, J. Lu, M. Qiu, *Laser Photonics Rev.* **2017**, *11*, 1700091.
- [30] J. Nag, R. F. Haglund Jr., *J. Phys.: Condens. Matter* **2008**, *20*, 264016.
- [31] N. Wang, S. Magdassi, D. Mandler, Y. Long, *Thin Solid Films* **2013**, *534*, 594.
- [32] P. Mandal, A. Speck, C. Ko, S. Ramanathan, *Opt. Lett.* **2011**, *36*, 1927.
- [33] I. Staudé, C. Rockstuhl, *Nat. Mater.* **2016**, *15*, 821.
- [34] S. Geiger, J. Michon, S. Liu, J. Qin, J. Ni, J. Hu, T. Gu, N. Lu, *ACS Photonics* **2020**, *7*, 2618.
- [35] X. Ni, Z. J. Wong, M. Mrejen, Y. Wang, X. Zhang, *Science* **2015**, *349*, 1310.
- [36] S. M. Kamali, A. Arbabi, E. Arbabi, Y. Horie, A. Faraon, *Nat. Commun.* **2016**, *7*, 11618.
- [37] X. Liu, J. Wang, L. Tang, L. Xie, Y. Ying, *Adv. Funct. Mater.* **2016**, *26*, 5515.
- [38] S. I. Park, D. S. Brenner, G. Shin, C. D. Morgan, B. A. Copits, H. U. Chung, M. Y. Pullen, K. N. Noh, S. Davidson, S. J. Oh, J. Yoon, K. I. Jang, V. K. Samineneni, M. Norman, J. G. Grajales-Reyes, S. K. Vogt, S. S. Sundaram, K. M. Wilson, J. S. Ha, R. Xu, T. Pan, T. i. Kim, Y. Huang, M. C. Montana, J. P. Golden, M. R. Bruchas, R. W. Gereau, J. A. Rogers, *Nat. Biotechnol.* **2015**, *33*, 1280.
- [39] H. Jing, R. Peng, R.-M. Ma, J. He, Y. Zhou, Z. Yang, C.-Y. Li, Y. Liu, X. Guo, Y. Zhu, D. Wang, J. Su, C. Sun, W. Bao, M. Wang, *Nano Lett.* **2020**, *20*, 7144.
- [40] S. Aikio, J. Hiltunen, J. Hiitola-Keinanen, M. Hiltunen, V. Kontturi, S. Siitonen, J. Puustinen, P. Karioja, *Opt. Express* **2016**, *24*, 2527.
- [41] C. A. Barrios, *Sensors* **2016**, *16*, 1643.
- [42] H. S. Ee, R. Agarwal, *Nano Lett.* **2016**, *16*, 2818.
- [43] S. C. Malek, H. S. Ee, R. Agarwal, *Nano Lett.* **2017**, *17*, 3641.
- [44] J. Brandrup, E. H. Immergut, E. A. Grulke, A. Abe, D. R. Bloch, *Polymer Handbook*, Wiley, NY, USA **1999**.
- [45] S. Yang, M. Vaseem, A. Shamim, *Adv. Mater. Technol.* **2019**, *4*, 1800276.
- [46] C.-I. Li, J.-C. Lin, H.-J. Liu, M.-W. Chu, H.-W. Chen, C.-H. Ma, C.-Y. Tsai, H.-W. Huang, H.-J. Lin, H.-L. Liu, P.-W. Chiu, Y.-H. Chu, *Chem. Mater.* **2016**, *28*, 3914.
- [47] Y. Chen, L. Fan, Q. Fang, W. Xu, S. Chen, G. Zan, H. Ren, L. Song, C. Zou, *Nano Energy* **2017**, *31*, 144.
- [48] J.-Y. Chae, D. Lee, D. W. Lee, H.-Y. Woo, J. B. Kim, T. Paik, *Appl. Surf. Sci.* **2021**, *545*, 148937.
- [49] W. Liang, Y. Jiang, J. Guo, N. Li, W. Qiu, H. Yang, Y. Ji, S.-N. Luo, *Adv. Opt. Mater.* **2019**, *7*, 1900647.
- [50] Q. Lu, M. Gao, C. Lu, T. Pan, T. Cheng, F. Long, Y. Lin, *J. Sol-Gel Sci. Technol.* **2021**, *98*, 24.
- [51] X. Deng, Y.-F. Zhao, N. Zhong, F.-Y. Yue, R. Huang, H. Peng, X.-D. Tang, P.-H. Xiang, Y.-H. Chu, C.-G. Duan, *Adv. Electron. Mater.* **2020**, *6*, 1900742.
- [52] T. Chang, Y. Zhu, J. Huang, H. Luo, P. Jin, X. Cao, *Sol. Energy Mater. Sol. Cells* **2021**, *219*, 110799.
- [53] D. H. Jung, H. S. So, J. S. Ahn, H. Lee, N. T. T. Thu, S. Yoon, S. Y. Kim, H.-Y. Jung, *J. Vac. Sci. Technol., A* **2018**, *36*, 03E102.
- [54] K. Han, L. Wu, Y. Cao, H. Wang, C. Ye, K. Huang, M. Motapothula, H. Xing, X. Li, D.-C. Qi, X. Li, X. Renshaw Wang, *ACS Appl. Mater. Interfaces* **2021**, *13*, 16688.
- [55] S. M. Ke, C. Chen, N. Q. Fu, H. Zhou, M. Ye, P. Lin, W. X. Yuan, X. R. Zeng, L. Chen, H. T. Huang, *ACS Appl. Mater. Interfaces* **2016**, *8*, 28406.
- [56] Z. Ma, V. Skumryev, M. Gich, *Mater. Adv.* **2020**, *1*, 1464.
- [57] O. A. Bauchau, J. I. Craig, *Structural Analysis*, Springer, Dordrecht **2009**.
- [58] H.-T. Kim, B.-G. Chae, D.-H. Youn, G. Kim, K.-Y. Kang, *Appl. Phys. Lett.* **2005**, *86*, 242101.
- [59] F.-Z. Shu, L.-H. Zhang, J.-N. Wang, R.-W. Peng, R.-H. Fan, D.-X. Qi, M. Wang, *Opt. Lett.* **2019**, *44*, 2752.
- [60] H. W. Verleur, A. S. Barker Jr., C. N. Berglund, *Phys. Rev.* **1968**, *172*, 788.
- [61] R. Lopez, T. Haynes, L. Boatner, L. C. Feldman, R. Haglund Jr., *Phys. Rev. B* **2002**, *65*, 224113.
- [62] N. Liu, M. Mesch, T. Weiss, M. Hentschel, H. Giessen, *Nano Lett.* **2010**, *10*, 2342.
- [63] W. Yu, Y. Lu, X. Chen, H. Xu, J. Shoo, X. Chen, Y. Sun, J. Hao, N. Dai, *Adv. Opt. Mater.* **2019**, *7*, 1900841.
- [64] E. Hecht, *Optics*, Addison Wesley, NY, USA **2002**.
- [65] A. K. Majumdar, J. C. Ricklin, *Free-Space Laser Communications: Principles and Advances*, Springer Science & Business Media LLC, NY, USA **2010**.